# Transient response of a submerged fluid-coupled double-walled shell structure to a pressure pulse[a)]

H. C. Neilson, G. C. Everstine, and Y. F. Wang

*David Taylor Naval Ship Research and Development Center, Bethesda, Maryland 20084*
(Received 8 May 1981; accepted for publication 2 September 1981)

A solution is presented for the interactive transient response of a submerged double-walled elastic sphere, flooded between the walls, to a plane step pressure pulse, using the general purpose finite element structural analysis computer program NASTRAN with the doubly asymptotic approximation (DAA) for external surface interaction loading and explicitly modeled fluid finite elements for between-wall coupling. The methods used are described and problems encountered in implementation are discussed, along with approaches used in overcoming them. Results are compared with an available exact solution for the same configuration, and with exact and approximate solutions for the inner shell as a stand-alone submerged structure. The comparisons indicate generally satisfactory results, verifying the applicability of these methods for a submerged, double-walled structure. In addition, the double-single shell comparisons suggest a hitherto untried means of improving the later-time accuracy of a finite element/DAA computation for a single-walled submerged structure by including in the structural model a few layers of fluid finite elements adjacent to the outer surface, and applying the DAA loading at the outer surface of this fluid envelope.

PACS numbers: 43.20.Rz, 43.20.Tb

## INTRODUCTION

The problem of the transient interaction between a pressure wave and a submerged elastic structure is of continuing interest. It is amenable to more or less exact solution only in certain special cases, chiefly exemplified in work of Huang,[1,2] who has applied classical techniques of separation of variables and Laplace transforms to obtain convergent series solutions. On the other hand, approximate methods, though less precise, can be more generally applicable, while the availability of exact solutions for certain special configurations provides a basis for evaluation of a given approximation technique.

The current state of the art in approximate methods is represented by finite element structural analysis with the doubly asymptotic approximation (DAA) of Geers.[3,4] Considerable success has been achieved at DTNSRDC utilizing the widely available general purpose finite element program NASTRAN in this way.[5,6]

The present paper details the application of these techniques to an otherwise simple submerged structure having the added complication of a contained fluid volume, requiring explicit finite element modeling of the contained fluid. Methods of accomplishing this are described and discussed, and time histories of computed responses are presented and compared with other solutions, both exact and approximate.

## I. PROBLEM DESCRIPTION

The configuration studied is shown in Fig. 1. In fact, it is the same configuration previously solved by Huang[2] using integral transform methods, thus facilitating the evaluation of the present approximate methods.

The structure is a double-walled steel shell construction, submerged in water and flooded between the walls. The geometric proportions and material properties are taken from the dimensionless parameters used by Huang. In proportional units $(a_i, \rho a_i^3, a_i/c)$ they are

inner shell middle surface radius

$$a_i = 1.0$$

outer shell middle surface radius

$$a_o = 1.25$$

inner shell thickness

$$h_i = 0.02$$

outer shell thickness

$$h_o = 0.005$$

mass density of fluid

$$\rho = 1.0$$

sound speed in fluid

$$c = 1.0$$

mass density of shells

$$\rho_s = 7.78846$$

Young's modulus of shells

$$E_s = 96.977$$

Poisson's ratio of shells

$$\nu_s = 0.3$$

The structure is impinged upon by a plane wave having the waveform of a unit step pressure pulse, again, as in Huang. Solution with the unit step incidence immediately establishes the response to impingement by a discontinuous wave front, and, once in hand, can be used to determine the response to any waveform through convolution integration.

[a)] All opinions or assertions made in this paper are those of the authors and are not to be construed as official or necessarily the views of the Navy or the naval service at large.

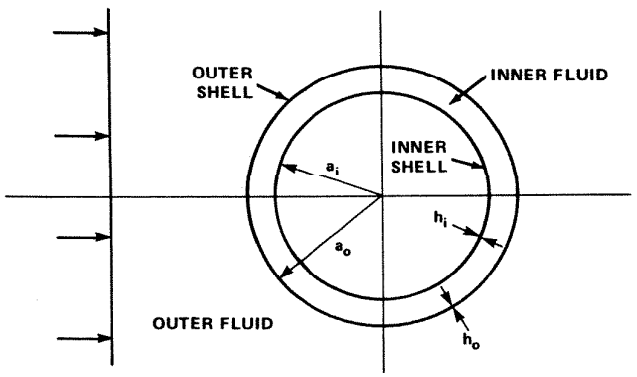


FIG. 1. Problem configuration.

## II. FORMULATION

The development described herein essentially follows the general methods previously presented by Everstein,[5,6] adapted and specialized as needed to the present problem configuration. Briefly stated this approach involves applying the direct transient integration capability of the finite element structural analysis computer program NASTRAN, modeling both structure and contained fluid with finite elements and using the doubly asymptotic approximation (DAA) of Geers[3,4] for supplying the external scattered pressure.

The general matrix form of the equations of motion which are integrated by NASTRAN is[7]

$$\mathbf{M}\ddot{\mathbf{u}} + \mathbf{B}\mathbf{u} + \mathbf{K}\mathbf{u} = \mathbf{F}\,. \tag{1}$$

Viewing the inner shell, inner fluid, outer shell, and outer fluid as four separate "structures," coupled only at the interfaces, and labeled 1, 2, 3, and 4, respectively, a matrix equation of the form of (1) can be set up for each, with internal degrees of freedom on the left-hand side and forcing functions on the right. For shell structures 1 and 3 these are straightforward and can be written as[5]

$$\mathbf{M}_1\ddot{\mathbf{u}}_1 + \mathbf{K}_1\mathbf{u}_1 = -\mathbf{A}_{1/2}\dot{\mathbf{q}}_2\,, \tag{2}$$

$$\mathbf{M}_3\ddot{\mathbf{u}}_3 + \mathbf{K}_3\mathbf{u}_3 = \mathbf{A}_{3/2}\dot{\mathbf{q}}_2 - \mathbf{A}_{3/4}\dot{\mathbf{q}}_4 - \mathbf{A}_{3/4}\mathbf{p}_i\,, \tag{3}$$

where $\mathbf{u}_j$ is the vector of grid point displacements of structure $j$, $\mathbf{M}_j$ and $\mathbf{K}_j$ are the lumped mass and stiffness matrices, respectively, of structure $j$, $\mathbf{A}_{j/k}$ is a matrix of area components converting pressures in fluid region $k$ to forces on shell structure $j$, $\mathbf{p}_i$ is the time dependent vector of incident free-field pressure in the external fluid (region 4), and $\dot{\mathbf{q}}_k$ is the vector of scattered or interaction pressures $p_s$ at grid points in fluid region $k$; i.e., $p_{\text{total}} = p_i + p_s$ at all points. The scattered fluid pressure variable $p_s$ has been replaced by a new variable $q$, essentially the scattered velocity potential in the fluid, defined so that $\dot{q} = p_s$. This is done to avoid the numerical problem of a Dirac delta, which is otherwise required in the fluid equations because of the discontinuous incident pressure wave front.

It has been shown[5] that the fluid dynamic responses can also be represented in discretized form by sets of linear differential equations in the scattered velocity potential $q$, having the general matrix form

$$\mathbf{Q}\ddot{\mathbf{q}} + \mathbf{D}\dot{\mathbf{q}} + \mathbf{H}\mathbf{q} = \mathbf{G}\,, \tag{4}$$

identical to that of Eq. (1). Consequently, utilizing one displacement degree of freedom at each fluid grid point to represent scattered velocity potential and constraining the other five to zero, the fluid Eq. (4) can be solved simultaneously with the structure Eqs. (1) by NASTRAN if the analog fluid inertia, damping, stiffness, and forcing matrices (Q, D, H, and G, respectively) can be defined numerically to the program.

In the inner fluid region explicit finite element fluid modeling is used,[6] with fictitious material properties chosen so that the elasticity equation in the single displacement degree of freedom remaining at a fluid grid point becomes identical numerically to the wave equation. This condition will be fulfilled by any combination of input material properties $\rho_e$, $G_e$, and $\nu_e$ such that

$$[2(1-\nu_e)]/(1-2\nu_e) = 1 \tag{5}$$

and

$$\rho_e/G_e = 1/c^2 \tag{6}$$

and compatible analog fluid inertia and stiffness matrices will be automatically computed by NASTRAN. Condition (5) is met numerically by letting

$$E_e = G_e \times 10^{20}\,, \tag{7}$$

causing the required value of $\nu_e$ to be computed internally. For convenience, condition (6) is met by choosing

$$G_e = 1/\rho\,, \tag{8}$$

so that

$$E_e = (1/\rho) \times 10^{20} \tag{9}$$

and

$$\rho_e = 1/\rho c^2\,. \tag{10}$$

With these values and the fluid–solid interface boundary conditions, the analog matrix equation of motion of the inner fluid (region 2) becomes

$$\mathbf{Q}_2\ddot{\mathbf{q}}_2 + \mathbf{H}_2\mathbf{q}_2 = \mathbf{A}^T_{1/2}\ddot{\mathbf{u}}_1 - \mathbf{A}^T_{3/2}\dot{\mathbf{u}}_3\,. \tag{11}$$

In the external fluid region the DAA is used for interactive pressure loading $p_s$. The basic matrix form of this approximate relation is

$$\dot{\mathbf{p}}_s + \rho c\,\mathbf{M}_a^{-1}\mathbf{A}\,\mathbf{p}_s = -\rho c\ddot{\mathbf{u}}_s\,, \tag{12}$$

where $\mathbf{M}_a$ is the added mass matrix for the outer shell (structure 3) submerged in the infinite external fluid (region 4), involving only surface normal degrees of freedom, and $\ddot{\mathbf{u}}_s$ is the vector of scattered wave particle accelerations normal to the structure surface and positive into the fluid. As applied in the velocity potential form[6] compatible with the equations of motion of the other three regions, and again incorporating fluid–solid interface boundary conditions this becomes

$$(1/\rho c)\mathbf{A}_{41}\dot{\mathbf{q}}_{41} + \mathbf{A}_{41}\mathbf{M}_a^{-1}\mathbf{A}_{41}\mathbf{q}_{41} = \mathbf{A}^T_{3/41}\dot{\mathbf{u}}_3 + (1/\rho c)\mathbf{A}_{41}p_i\cos\theta_{41}\,, \tag{13}$$

where set 41 is the set of fluid degrees of freedom at

the interface between shell structure 3 and fluid region 4, and $A_{41}$ is a diagonal matrix of area factors relating fluid interface degrees of freedom and surface normal interface degrees of freedom.

Equation (13) again is of the form of Eq. (4), with the inertia matrix $\mathbf{Q}=0$, damping $D=(1/\rho c)A_{41}$, stiffness $H=A_{41}M_a^{-1}A_{41}$, and forcing functions $G=A_{3/41}^T\dot{u}_3+(1/\rho c)A_{41}p_i\cos\theta_{41}$. If the added mass matrix $\mathbf{M}_a$ is computed externally the stiffness H can be formed and input directly to NASTRAN. Alternatively, $M_a$ can be approximated by internal computation. It has been shown[6] that for a structure (3) submerged in a finite fluid region (4) with both (3) and (4) modeled with finite elements and with the set of structure surface normal interface degrees of freedom in one-to-one correspondence with the fluid interface degrees of freedom (set 41), the added mass matrix is given by

$$M_a=A_{41}(H'_{41})^{-1}A_{41}\,, \tag{14}$$

if the fluid stiffness matrix $H_4$ (reduced by static condensation to $H'_{41}$) is assembled using fictitious fluid material properties

$$G_e=1/\rho\,, \tag{15}$$

and

$$E_e=10^{20}G_e=(1/\rho)\times 10^{20}\,, \tag{16}$$

and if each fluid grid point is limited to one unconstrained translational degree of freedom. Although the added mass matrix so constituted varies for different finite fluid regions with the same interface sets, it approaches the infinite fluid region matrix if the outer fluid boundaries (where $p=0$) are sufficiently far[6] from the structure.

With the internally computed fluid stiffness matrix $H_4$ internally condensed to $H'_{41}$ Eq. (13) becomes

$$(1/\rho c)A_{41}\dot{q}_{41}+H'_{41}q_{41}$$
$$=A_{3/41}^T\dot{u}_3+(1/\rho c)A_{41}p_i\cos\theta_{41}\,, \tag{17}$$

where also the fictitious element mass density $\rho_e=0$ is used to nullify the automatically computed inertia matrix Q. Alternatively, Eq. (17) can be expanded to include all unconstrained degrees of freedom of the finite external fluid region,

$$(1/\rho c)A_4\dot{q}_4+H_4q_4=A_{3/4}^T\dot{u}_3+(1/\rho c)A_4p_i\cos\theta_4\,, \tag{18}$$

since all coefficient matrices $A_{j/k}$ have nonzero entries only at intersections of rows and columns corresponding to interface degrees of freedom. $H_4$ is then the uncondensed fluid stiffness matrix of the external fluid (region 4).

Equations (2), (3), (11), and (17) together now represent a system of equations which is again of the form of matrix Eq. (1), and which can be represented symbolically in partitioned form as in Eq. (19).

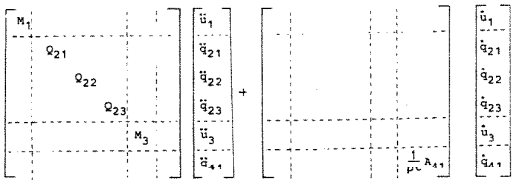

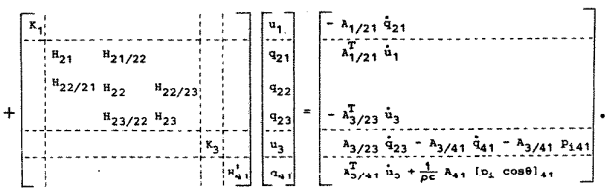

(19)

Here set 21 is the set of inner fluid degrees of freedom at the interface between shell structure 1 and fluid region 2, and set 23 is the set of inner fluid degrees of freedom at the interface between shell structure 3 and fluid region 2, while set 22 contains the remaining, noninterface, inner fluid degrees of freedom. In this form the fluid and structural partitions are uncoupled on the left-hand side, all coupling occurring through velocity dependent loading terms on the right-hand side. In using this form the grid point numerical sequencing is chosen to maintain the uncoupled partitions on the left-hand side and the condensed fluid stiffness matrix $H'_{41}$ (small and full) is used, to minimize matrix size and bandwidth. Difficulties have been experienced in achieving numerical stability using this form in the present problem.

Alternatively, the velocity dependent loading terms can be moved to the left-hand side as coupling terms in the damping matrix Eq. (20).

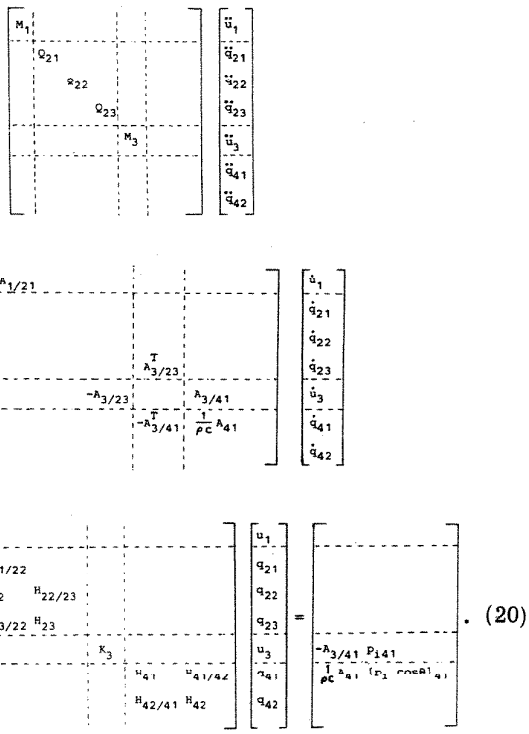

(20)

Now only the time dependent incident pressure loading terms remain on the right-hand side, and the numerical time integration by NASTRAN is inherently stable.[7] Other numerical advantages are lost in the process, however, in the increased bandwidth of the coefficient matrix due to increased coupling on the left-hand side and in the loss of symmetry in the damping matrix, somewhat balancing the increased time step size per-

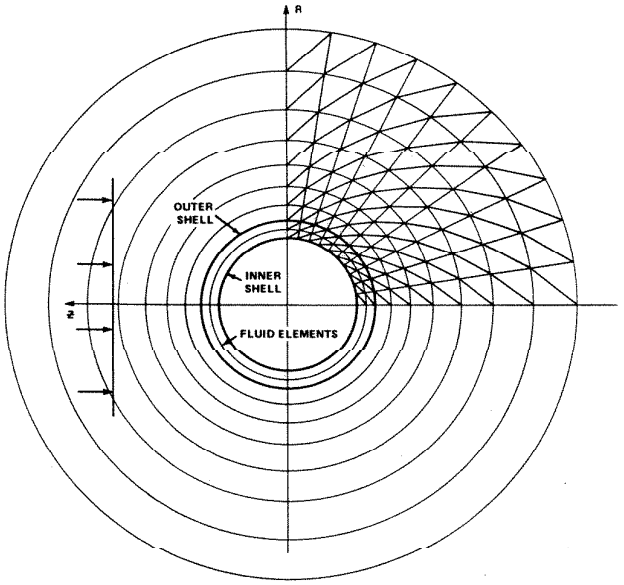


FIG. 2. Finite element model 1.

missible. In using this form the grid points are sequenced to minimize the overall bandwidth, and the uncondensed stiffness matrix of the external fluid region

$$H_4 = \begin{bmatrix} H_{41} & H_{41/42} \\ H_{42/41} & H_{42} \end{bmatrix} \tag{21}$$

is used. The 4/4 partition is therefore large and sparse. Both of these alternative forms have been applied to the present problem.

## III. IMPLEMENTATION

Although not required by the method or by NASTRAN, which is a general purpose structural analysis program, the economies of symmetry were exploited where possible in the present problem, due to axial symmetry of both the structure and the loads, and therefore of the expected responses. The axisymmetric element capability of NASTRAN was employed,[8] with a two-dimensional mesh of ring nodes established by RINGAX cards, as indicated in Figs. 2 and 3. The shell structures were modeled with CONEAX axisymmetric conical shell elements, and the fluid regions with TRIAAX axisymmetric solid elements. Time dependent loads were applied via TLOAD 1, DAREA, and DELAY cards, and velocity dependent loads by the nonlinear load card type NOLIN 1. The fictitious damping matrix was entered directly via the DMIG card type. The inertia and stiffness matrices were computed internally by NASTRAN, in the case of the fluid partitions with fictitious material properties entered via the MAT1 card type. For region 2 (internal fluid) these are

$$G_e = 1.0,$$
$$E_e = 1.0 \times 10^{20},$$
$$\rho_e = 1.0,$$

and for region 4 (external fluid)

$$G_e = 1.0,$$
$$E_e = 1.0 \times 10^{20},$$
$$\rho_e = 0.0.$$

Static condensation of the external fluid stiffness partition $H_4$, where appropriate, was accomplished by way of the OMITAX card type.

The axial translational degree of freedom (dof 3) was used as the potential analog degree of freedom in the fluid regions.[6] All other degrees of freedom of all fluid ring nodes were constrained to zero, and at the external fluid outer boundary the dof 3's were also constrained as per the outer boundary condition $q = 0$. The circumferential translational (dof 2), radial rotational (dof 4), and axial rotational (dof 6) degrees of freedom of all shell ring nodes were constrained because of axial symmetry of the loading and therefore of the responses.

The outer boundary of the external fluid, where all fluid degrees of freedom were constrained to zero, was taken to be spherical and set at a radius of approximately 4.2, or roughly 3.4 times the radius of the outer spherical shell, a proportion previously demonstrated to place the boundary sufficiently far from a spherical structure for valid use of Eq. (19) or (20).

The initial attempt at a solution was made in the form of Eq. (19), that is with right-hand-side coupling using velocity dependent loads, and condensed external fluid stiffness partition $H'_{41}$. The finite element modeling was as shown in Fig. 2, designated model 1, with 20 equal angular divisions between the positive and negative poles, two geometrically progressive radial divisions in the inner fluid, and seven in the external

TABLE I. Computational statistics.

| Finite element model | Formulation | No. of ring nodes | No. of solution set dof's | Time step ($\Delta T$) | No. of time steps | CDC 6400 cpu time (s) |
|---|---|---|---|---|---|---|
| 1 | 19 (RHS coupling) | 273 | 202 | 0.05 | 406 | 1200 |
| | | | | 0.025 | 812 | 1900 |
| | | | | 0.0125 | 1624 | 3200 |
| | | | | 0.00625 | 3248 | 5900 |
| | 20 (LHS coupling) | 273 | 328 | 0.1 | 203 | 1001 |
| | | | | 0.05 | 406 | 2017 |
| 2 | 20 | 558 | 643 | 0.1 | 203 | 2930 |

fluid region. The ring node numerical sequencing was by (1) region (1,2,3,4), (2) angular location (1 to 21), and (3) radial location within the region, thus maintaining the uncoupled structure and fluid partitions on the left-hand side of Eq. (19). Finally, the time step size used for numerical integration was $\Delta T = 0.05$ or 1/20 of the radial transit time, i.e., the time required for the wave front to travel the distance of the middle-surface radius of the inner sphere.

The above characteristics were chosen on the basis of a previous successful NASTRAN/DAA solution of a submerged single-walled spherical shell physically identical to the inner shell of the present configuration. However, in the double-sphere case severe instability was encountered in the computed results. Three additional runs were then made, each with the same modeling and formulation but with the time step reduced by half from the previous run, the final run thus using a time step $\Delta T = 0.00625$. With each reduction in time step the magnitude of the instability oscillations was greatly reduced, but never disappeared entirely, while the computation time increased sharply (Table I).

The problem was then reformulated in accordance with Eq. (20), that is with left-hand-side coupling and using the uncondensed external fluid stiffness partition $H_4$. The finite element representation remained model 1, again as shown in Fig. 2, but with the ring nodes sequenced according to (1) angular location, (2) region (1,2,3,4), and (3) radial location within the region, in order to minimize the overall matrix bandwidth and wave front. This mathematical configuration was then run with time steps of 0.05 and 0.1. In both cases the results showed no tendency toward instability over the time span of the computation, as expected, since the loading at any point was now exclusively time dependent. Also, computation times were reduced considerably from those for the best results using right-hand-side coupling (Table I). However, some extraneous, evidently purely numerical distortion of the computed results was still apparent, indicating that refinement of the finite element model was needed. Chiefly suspect was the modeling of the inner fluid region, where no more than two radial divisions could be made with the 20 equal angular divisions without excessive elongation of the fluid element cross sections.

The physical configuration was then remodeled as shown in Fig. 3, with 30 equal angular divisions between the positive pole (0°) and the negative pole (180°), allowing three geometrically progressive radial divisions in the inner fluid and 11 in the external fluid region. The problem formulation indicated by Eq. (20) was again used, with left-hand-side coupling and uncondensed external fluid stiffness partition $H_4$. The ring node numerical sequencing was the same as previously indicated for left-hand-side coupling with model 1. The time step used for this final configuration was $\Delta T = 0.1$.

## IV. RESULTS AND DISCUSSION

Representative final results are shown graphically in terms of relative axial displacement between the apexes of the inner shell in Fig. 4 and in terms of inner shell velocity components in Figs. 5 through 9. Preliminary results from the present investigation are included in Figs. 5 and 6 for comparison purposes. Likewise, relative displacements taken from the series solution of the double-walled configuration[2] are included in Fig. 4, and velocity components from previous series[1] and NASTRAN/DAA solutions of the corresponding single-walled configuration are included in Figs. 7–9. Note that in Fig. 4 the zero of time is the wave-front arrival time at the $Z$ location of the positive pole of the inner sphere, while in Figs. 5 through 9 it is the initial impingement time of the outer sphere.

Examining the progressions of results in Figs. 5 and 6 through the previously described sequence of modelings and formulations, limiting tendencies appear to

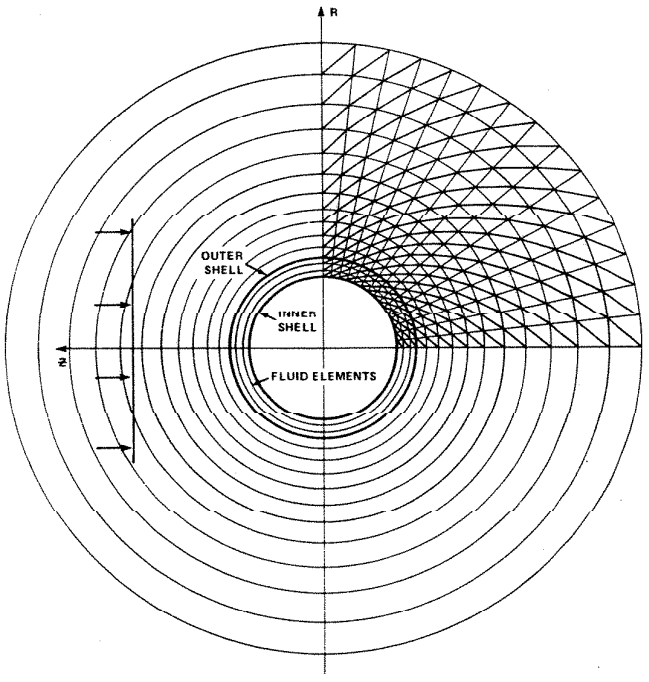


FIG. 3. Finite element model 2.

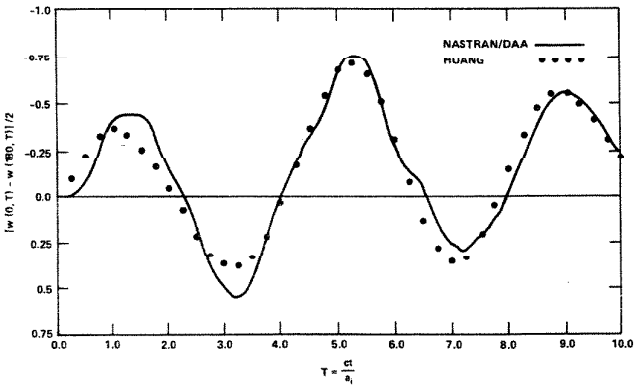


FIG. 4. Relative radial displacement between positive and negative poles of inner sphere.

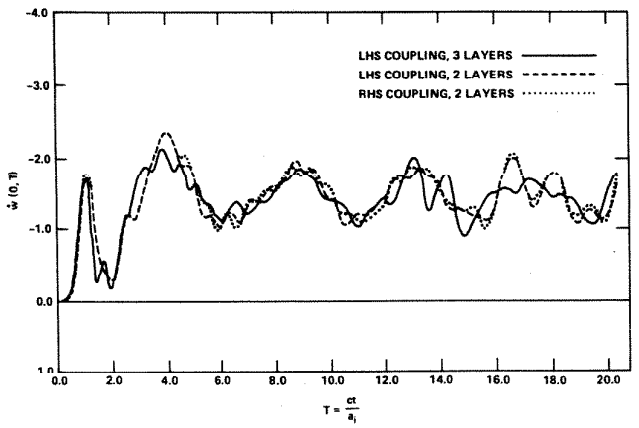


FIG. 5. Radial velocities of positive pole of inner sphere for three mathematical configurations.

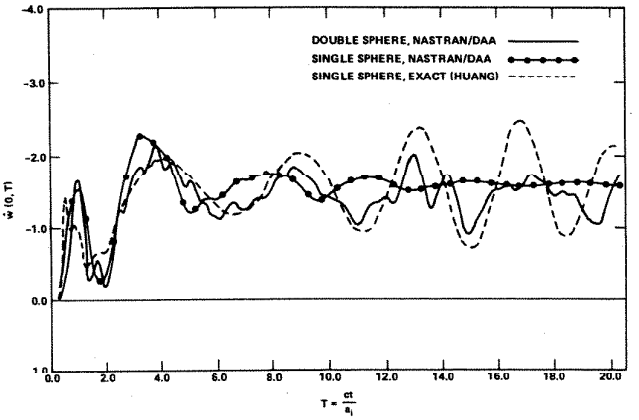


FIG. 7. Radial velocities of positive poles of inner sphere and single sphere.

exist, but to be subject to modeling-dependent numerical distortion, indicating that even further refinement of the model might be beneficial in terms of accuracy of the results. However, the computational costs of such refinement increase rapidly, as can be seen in Table I. In any practical application therefore the degree of accuracy and resolution desired or required must be considered in terms of the computational costs entailed, a common situation in finite element analyses.

Note that computational costs of the final run (Table I) could be roughly halved without loss of accuracy by symmetrizing the coefficient matrices on the left-hand side of Eq. (20), since in NASTRAN the computational load is reduced for symmetric matrix operations. The stiffness matrix is then no longer positive definite, and minor program changes in NASTRAN are required to accept the unorthodox data input, i.e., negative material properties for the fluid regions. The requisite program changes have in fact been incorporated in the DTNSRDC version of NASTRAN since the completion of these analyses.

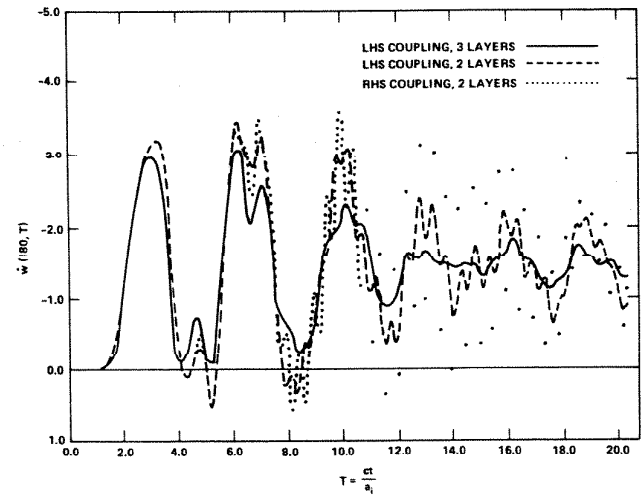


FIG. 6. Radial velocities of negative pole of inner sphere for three mathematical configurations.

The NASTRAN/DAA relative displacement results plotted in Fig. 4 are those of the final run, using the refined finite element model and left-hand-side coupling. The "exact" results plotted are the series solution of Huang,[2] and agreement is obviously quite good over the time span available for comparison, which was limited to ten radial transit times.

It has been shown[2] that in the present configuration the effects of the relatively thin outer shell on the inner shell responses are small, consisting mainly of a slight overall lowering of a given response curve for the unshielded inner sphere while maintaining its shape and periodicity. Additional comparisons were therefore made, in terms of inner shell velocity components, between the present results and previous series solution[1] and NASTRAN/DAA single-sphere results (Figs. 7–9), which were available in greater quantity than the double-sphere results and for a span of 20 radial transit times. The single-walled configuration was physically identical to the inner shell of the double-walled configuration, lacking only the shielding outer sphere.

Qualitatively, these comparisons seem to bear out the previous conclusion that the present results are subject to modeling-dependent numerical distortion.

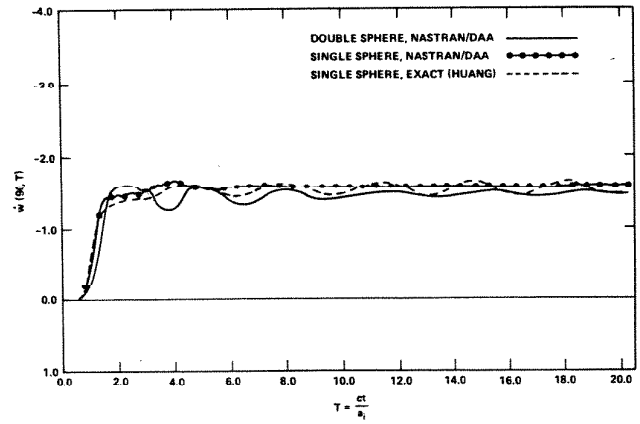


FIG. 8. Tangential velocities of equators of inner sphere and single sphere.

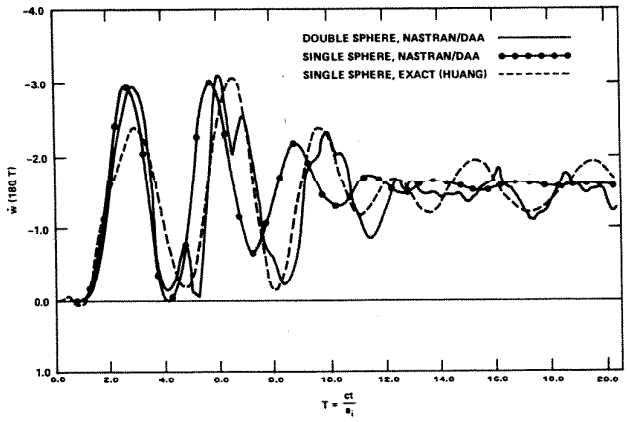


FIG. 9. Radial velocities of negative poles of inner sphere and single sphere.

However, again qualitatively, the comparisons seem to indicate intrinsic shapes and periodicities in the present results which more closely resemble those of the series solution single-sphere results then of the NASTRAN / DAA single sphere results, especially in the intermediate time range from about 4 to 12 radial transit times. Conjecturing as to possible causes of this apparent phenomenon, the DAA is generally regarded as producing good results at early times in fluid-structure interaction problems, but providing somewhat excessive damping of structure responses at later times. An alternative technique is described by Everstine,[6] comprising explicit finite element modeling of a finite volume of fluid external to the structure, with application of an appropriate radiation condition at the outer fluid boundary. The present analysis utilized explicit finite element modeling of a small fluid volume external to the inner shell and applied the DAA to the outer boundary of this fluid region through the thin outer shell, which is virtually transparent to the incoming wave.[2] Effectively, a small volume of fluid modeled "exactly" (in a finite element sense) was interposed between the structure (the inner shell) and the damping effect of the DAA leading, at least conjecturally, to the apparent phenomenon described above.

Conjecturing further, this suggests that the outer shell elements might be removed entirely, the DAA then becoming the desired approximate radiation condition on the outer boundary of the inner fluid. This in turn suggests deliberate application as an alternative computational stratagem in a fluid-structure interaction problem if more detailed resolution of structure responses, particularly in the intermediate time ranges, is required to the extent that the added computational effort is warranted; that is, modeling a few layers of fluid finite elements external to the structure surface and applying the DAA at the outer boundary of the fluid volume modeled.

## V. SUMMARY

A double-walled steel shell structure, submerged in water and flooded between the walls, has been analyzed using the general purpose finite element computer program NASTRAN, with explicit finite element modeling of the contained fluid and approximation of the external fluid-structure interaction effects by the DAA. Numerical results compare favorably with a previous series solution of the same submerged structure, although subject to apparent modeling-dependent numerical distortion. Comparisons with single-sphere solutions, both by classical and finite element/DAA techniques, have suggested a possible alternative solution technique in general structure-fluid interaction problems; namely explicit finite element modeling of a relatively small volume of fluid external to the submerged structure, with the DAA utilized as the approximate radiation condition on the outer fluid boundary.

[1]H. Huang, "Transient Interaction of Plane Acoustic Waves with a Spherical Elastic Shell," J. Acoust. Soc. Am. 45, 661–670 (1969).
[2]H. Huang, "Transient Response of Two Fluid-Coupled Spherical Elastic Shells to an Incident Pressure Pulse," J. Acoust. Soc. Am. 65, 881–887 (1979).
[3]T. L. Geers, "Residual Potential and Approximate Methods for Three-Dimensional Fluid-Structure Interactions Problems," J. Acoust. Soc. Am. 49, 1505–1510 (1971).
[4]T. L. Geers, "Doubly Asymptotic Approximation for Transient Motions of Submerged Structures," J. Acoust. Soc. Am. 64, 1500–1508 (1978).
[5]G. C. Everstine, E. A. Schroeder, and M. S. Marcus, "The Dynamic Analysis of Submerged Structures," NASTRAN: User's Experiences, NASA TM X-3278, 419–429 (September 1975).
[6]G. C. Everstine, "A NASTRAN Implementation of the Doubly Asymptotic Approximation for Underwater Shock Response," NASTRAN: User's Experiences, NASA TM X-3428, 207–228 (October 1976).
[7]*The NASTRAN Theoretical Manual* [NASA SP-221(03), Washington, DC, March 1976].
[8]*The NASTRAN User's Manual* [NASA SP-222(03), Washington, DC, March 1976].